Observation of a Fragmented, Strongly Interacting Fermi Gas

Sebastian Krinner, David Stadler, Jakob Meineke, Jean-Philippe Brantut,* and Tilman Esslinger
Department of Physics, ETH Zurich, 8093 Zurich, Switzerland

(Received 10 February 2015; revised manuscript received 18 April 2015; published 22 July 2015)

We study the emergence of a fragmented state in a strongly interacting Fermi gas subject to a tunable disorder. We investigate its properties using a combination of high-resolution *in situ* imaging and conductance measurements. The fragmented state exhibits saturated density modulations, a strongly reduced density percolation threshold, lower than the average density, and a resistance equal to that of a noninteracting Fermi gas in the same potential landscape. The transport measurements further indicate that this state is connected to the superfluid state as disorder is reduced. We propose that the fragmented state consists of unpercolated islands of bound pairs, whose binding energy is enhanced by the disorder.

DOI: 10.1103/PhysRevLett.115.045302 PACS numbers: 67.85.De, 05.60.Gg, 37.10.Gh, 67.10.Jn

The concept of fragmentation has been introduced to extend the description of Bose-Einstein condensation to situations when low-energy states become degenerate. This condition can be achieved using internal atomic states, momentum states in one-dimensional gases, or angular momentum states in rotating gases. In real space, fragmentation occurs in multiple well geometries, including optical lattices [1]. In random potentials, fragmentation can manifest itself as a glassy state [2,3] and has been studied experimentally using ultracold bosonic gases [4–8]. Fermionic quantum gases differ from their bosonic counterparts in that the presence of spatial inhomogeneities directly affects the pairing mechanism via confinement-induced effects [9]. Consequently, pairing is an additional mechanism by which disorder can influence superfluidity and the occurrence of fragmentation. This is also discussed for solid-state materials, where strongly inhomogeneous materials show superconductor-to-insulator transitions [10].

In this Letter, we present the observation of a fragmented state of a strongly interacting Fermi gas, formed by tightly confining a unitary gas along one direction and exposing it to a microscopic disorder. Specifically, we start with a Fermi gas containing $9.9(7) \times 10^4$ atoms in each of the two lowest hyperfine states prepared in a homogeneous magnetic field of 834 G where the s-wave scattering length diverges, resulting in a superfluid with short coherence length [11]. The thin film is created by strongly confining the gas along one direction using a suitably shaped off-resonant laser beam. In addition, two high-resolution microscopes are used to optically project a controlled disorder potential into the two-dimensional region and to image the atomic density distribution at a micrometer length scale. The confined section is connected to two larger trapping regions acting as reservoirs, allowing us to perform two-terminal conductance measurements [12–14].

The thin film has a chemical potential $\mu \simeq 1.9\hbar\omega_z = 0.55(7)\ \mu$K, where $\omega_z = 2\pi \times 6.1(2)$ kHz is the trap frequency along the tightly confined z direction. This yields an interaction parameter $\ln(k_\mu a_{2D}) = 1.4$ in the absence of disorder, corresponding to a strongly interacting BCS-type regime [15–17], with a_{2D} denoting the two-dimensional scattering length [30] and $k_\mu = \sqrt{2m\mu/\hbar^2}$ the momentum associated with the chemical potential. We add a controlled, repulsive disorder in the film [31] by projecting an optical speckle pattern at a wavelength of 532 nm through one of the microscope objectives. It can be imaged by the second microscope, allowing for a precise characterization of the disordered potential. The pattern has a Gaussian envelope with a waist of 35 μm and a correlation length $\sigma = 0.72(5)\ \mu$m, defined as the $1/\sqrt{e}$ radius of a Gaussian fit to the autocorrelation function. This introduces two new energy scales, the average disorder strength $\bar{V}$, defined as the ac Stark shift at the maximum of the envelope, and the correlation energy $E_\sigma = \hbar^2/m\sigma^2$. We have $\mu > E_\sigma$, so that Anderson localization of individual atoms at weak disorder should not occur [32,33]. However, we also have $E_\sigma = 2.4 \times E_b$, where $E_b = 0.24\hbar\omega_z$ is the binding energy of pairs in a unitary Fermi gas tightly confined along one direction [15,16], implying that disorder will exert different forces on the two paired constituents. In this regime, pairing is directly influenced by disorder even though the density within one well of the random potential may be sufficient to sustain superfluidity locally. A similar situation occurs in a granular superconductor with small grains [34].

We first investigate the density distribution in the disordered potential using high-resolution imaging. Starting from a strongly interacting gas in the channel, we switch on the disorder to a variable strength and wait for 150 ms for thermalization with the reservoirs. The atoms are then illuminated by a 4 μs pulse of resonant light with an intensity of about 0.1 I_{sat}, where I_{sat} is the saturation intensity of the atomic transition, and the absorption pattern is registered on an electron multiplied charge coupled device camera. Typically, we average 20 of those pictures to reduce noise, leading to the images shown in Fig. 1. All

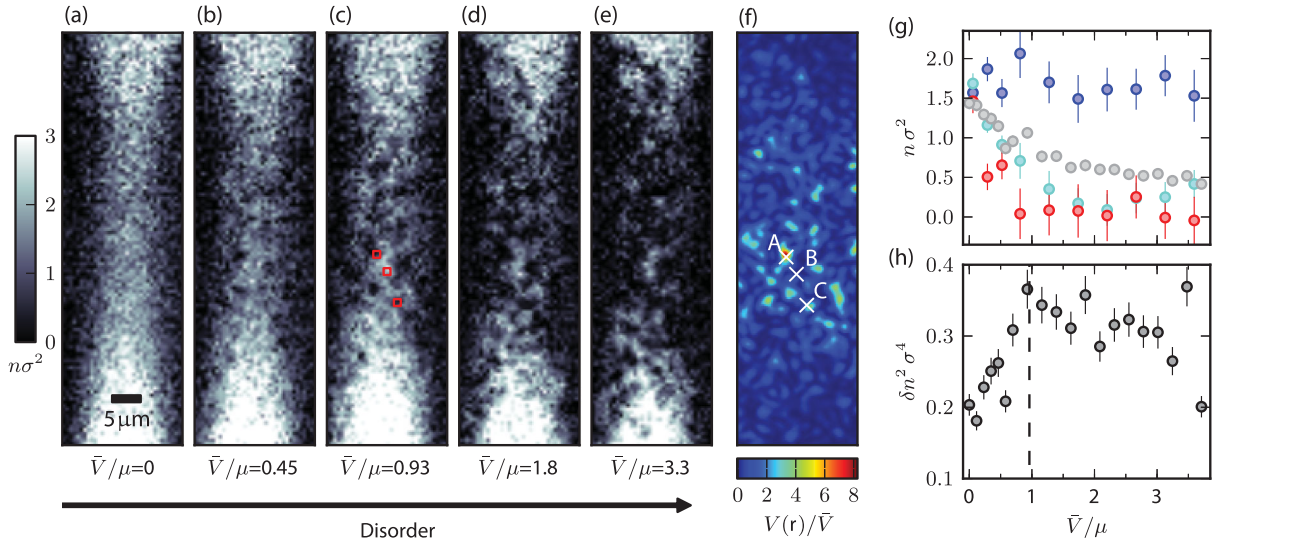

FIG. 1 (color). Evolution of the column density n (in units of σ^{-2}) as the disorder strength is increased. (a)–(e) High-resolution images of size 21 μm × 72 μm of the *in situ* density distribution in the channel for increasing $\bar{V}/\mu$. The saturated column density on top and bottom marks the beginning of the reservoirs, which extend far beyond the field of view. The systematic uncertainty in $\bar{V}/\mu$ is estimated to be 25%. (f) Image of the projected speckle pattern. The density ripples, gradually appearing from (a) to (e) can be matched one to one to bright (potential hills) and dark spots (potential valleys) in the image. (g) Local column density as a function of disorder strength for three specific points indicated in the potential landscape of (f) (point A, red; point B, blue; point C, cyan), each computed within a region of size 1.2 μm × 1.2 μm marked as red squares in (c). The gray data points are the mean column density in the channel, computed in a central region of size 18 μm × 7 μm. (h) Variance of the density computed in the same central region. The dashed line represents the theoretical percolation threshold for the potential seen by pointlike pairs.

subsequent analysis is performed on the averaged images and for one given realization of the disordered potential depicted in Fig. 1(f).

Figure 1(a) shows a clean film, smoothly connected on two sides to reservoirs; see Refs. [12,17] for details. For $\bar{V}/\mu = 0.45$ [Fig. 1(b)], first density ripples appear. With increasing $\bar{V}/\mu$, they become more pronounced until $\bar{V}/\mu = 1.8$ [Fig. 1(d)], where unpopulated regions occupy a significant fraction of the channel. At the largest disorder strength of $\bar{V}/\mu = 3.3$ [Fig. 1(e)], the gas is composed of disconnected pockets separated by large empty regions. Figure 1(f) shows the potential landscape observed directly with our imaging system (see the Supplemental Material [17]). In Fig. 1(g), the density at three distinct points [labeled A, B, C in Fig. 1(f)] is monitored along the fragmentation process. Points A and C correspond to a large and a moderate potential hill and the local densities at these positions decrease correspondingly fast. In contrast, point B corresponds to a potential valley and its local density remains constant, suggesting that the superfluid persists at this point for all disorder strengths. The density averaged over the center part of the channel is shown for comparison in the same graph. It shows a smooth decrease with increasing disorder, due to the repulsive nature of the random potential.

Density modulations are quantified by the variance of the density δn^2. $\delta n^2\sigma^4$ is presented in Fig. 1(h) as a function of disorder strength and shows a nonmonotonic evolution: from zero disorder to $\bar{V}/\mu \sim 1$, density modulations increase quickly although the average density decreases in this interval. Having reached its maximum value at around $\bar{V}/\mu \sim 1$, the modulations slowly decrease for higher disorder, likely because the average density decreases.

As the thin film fragments under the influence of disorder, the two reservoirs get gradually disconnected. Both thermodynamic and transport properties of the disordered thin film are a direct consequence of the ability of atoms to reach the reservoirs from the center of the film. Thermal equilibrium is ensured by atom exchanges between the film and the reservoirs [35,36]. Semiclassically, the density distribution reflects the distribution of allowed regions, suggesting that the properties of the film are related to the percolation properties of the density. We extract the latter by determining for each disorder strength the length l of the shortest possible connecting path from one reservoir to the other, along which the density n always stays above a certain density level $\tilde{n}$ (see the Supplemental Material [17]). The distance between the two ends of the reservoirs is $L = 42$ μm. A typical result is presented in Fig. 2(a).

We evaluate the normalized path length l/L as a function of $\tilde{n}$. The results are shown in Fig. 2(b) for different disorder strengths. Typically, l/L remains close to 1 for $\tilde{n}$ much smaller than the mean density since the path remains close to a straight line. With increasing $\tilde{n}$, l/L increases since regions of low density have to be circumvented. Beyond a critical threshold $\tilde{n} \geq n_{\mathrm{th}}$, no connecting path

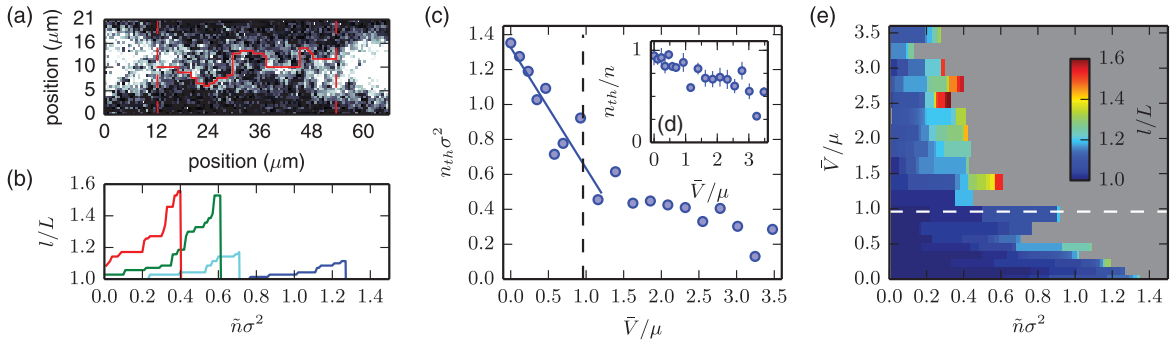

FIG. 2 (color). Percolation properties of the density distribution. (a) Shortest connecting path between the two ends of the reservoirs (indicated by the red dashed lines) for $\bar{V}/\mu = 1.39$ and a density level of $\tilde{n} = 0.6/\sigma^2$ close to the percolation threshold. The path displays strong deviations from a straight line and has a length of $1.5L$. (b) Shortest path length as a function of density level $\tilde{n}$ (in units of σ^{-2}), for $\bar{V}/\mu = 0.12, 0.58, 1.39, 2.78$ in blue, cyan, green, red, respectively. (c) Percolation threshold as a function of disorder strength. The solid line is a linear fit to the first 9 points. (d) Percolation threshold normalized to the average density as a function of disorder strength. Error bars represent the statistical error in the measurement of n. (e) Map of the relative path length as a function of $\tilde{n}$ and $\bar{V}/\mu$. The dashed lines in (c) and (e) represent the theoretical percolation threshold of the potential seen by pointlike pairs of atoms.

exists anymore. For large disorder strengths ($\bar{V}/\mu = 1.39, 2.78$), l/L reaches values as high as 1.6 for $\tilde{n}$ close to n_{th}, limited by the extension of the cloud in the transverse direction. In contrast, for low disorder strengths ($\bar{V}/\mu = 0.12, 0.58$), the increase is limited to $l/L \sim 1.2$, which is comparable to the detection-noise-induced increase without disorder (see the Supplemental Material [17]). These $l(\tilde{n})$ curves are typical for percolation transitions, and allow us to unambiguously identify the percolation threshold of the density n_{th}. The thresholds are plotted as a function of disorder strength in Fig. 2(c). Two regimes can be identified: for $\bar{V}/\mu < 1$, n_{th} shows a fast decrease, whereas for $\bar{V}/\mu > 1$, the decrease is slowed down. They correspond to the regimes of growing and saturated density modulations observed in Fig. 1(h).

The ratio of the percolation threshold to the mean density is presented in Fig. 2(d). It starts very close to 1 for weak disorder. This is expected since the percolation threshold of a 2D, continuous, symmetric, random variable is its mean [37]. For stronger disorder, the ratio drops well below 1. From this, we deduce that the density profile has become asymmetric; i.e., applied to our case, there are more empty regions than regions having an excess density.

The path length l/L as a function of disorder strength allows us to further characterize the system. To show this, we stack all $l(\tilde{n})/L$ curves as a function of disorder strength on the vertical axis, encoding l/L in color in Fig. 2(e). It is set to gray if no connecting path exists. The resulting 2D map is shown in Fig. 2(e), manifesting the two regimes also in the path length: for $\bar{V} < \mu$, the maxima of l/L reached at the percolation transitions remain moderate, whereas in the strongly disordered regime $\bar{V} > \mu$, large values of l/L are encountered. The transition observed in Figs. 2(c) and 2(e) coincides with the maximum in the density modulations in Fig. 1(h), confirming our interpretation of two regimes, smooth and fragmented. For comparison, we have reproduced the percolation analysis on a thin film subject to a homogeneous repulsive potential instead of the speckle pattern [13], finding only a single smooth regime (see the Supplemental Material [17]).

The evolution from smooth to fragmented density is accompanied by a clear change in the transport properties. We measure the dimensionless resistance r of the thin film as a function of disorder strength [13,14,17]. The results are presented in Fig. 3(a) and are similar to the case of a disordered bosonic superfluid [14]. For the lowest disorder, the resistance is below our measurement resolution, as it should be for a superfluid gas. The resistance increases very quickly until $\bar{V}/\mu \sim 0.7$. Above this disorder strength, the resistance increases more slowly. In order to disentangle the effects of strong interactions from single-particle effects, like simple atomic diffusion, we repeat the same experiment with a weakly interacting Fermi gas, for the same trapping potential, disorder configuration, and atom number. The measured resistances are shown in Fig. 3(a) as gray circles and show a smooth exponential evolution with disorder strength. For zero disorder, the resistance corresponds to the contact resistance of the ballistic channel [12].

We compare the transport properties of the two cases by evaluating the ratio of absolute resistances $R_{\mathrm{uni}}/R_{\mathrm{WIF}} = C_{\mathrm{WIF}}/C_{\mathrm{uni}} \times r_{\mathrm{uni}}/r_{\mathrm{WIF}}$, where C_{uni} (C_{WIF}) is the compressibility of the reservoirs for the unitary (weakly interacting) Fermi gas. Assuming zero temperature and a harmonic trap for unitary and weakly interacting Fermi gases, one obtains $C_{\mathrm{WIF}}/C_{\mathrm{uni}} = \sqrt{\xi_B}$, where $\xi_B = 0.38$ is the Bertsch parameter [38]. Figure 3(b) shows the evolution of $R_{\mathrm{uni}}/R_{\mathrm{WIF}}$ with disorder strength. We observe a sharp decrease for $\bar{V}/\mu < 0.7$. Interestingly, in the strong disorder regime at $\bar{V}/\mu \gtrsim 1$, $R_{\mathrm{uni}}/R_{\mathrm{WIF}}$ varies only weakly and remains close to 1. This suggests that beyond a certain disorder strength,

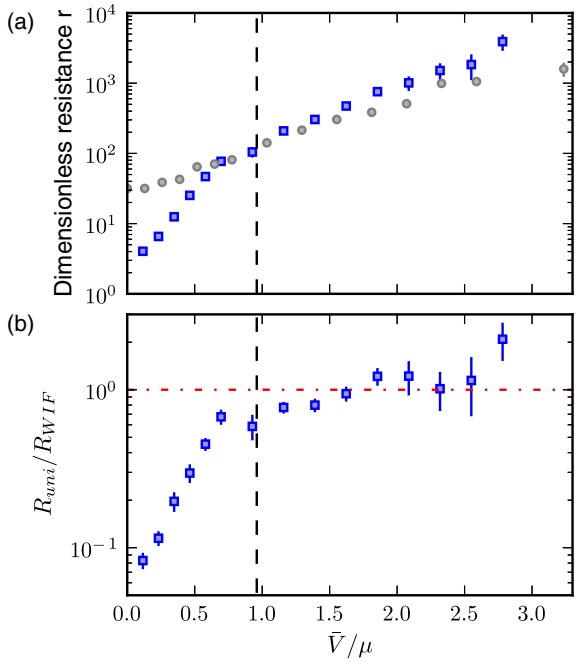

FIG. 3 (color online). Resistance of the thin film. (a) Dimensionless resistance as a function of disorder strength for the strongly interacting Fermi gas (blue squares) and for a weakly interacting Fermi gas (gray circles) for comparison. (b) Ratio of absolute resistances of the strongly and weakly interacting Fermi gas. The dash-dotted horizontal red line emphasizes that the ratio is close to 1 in the strongly disordered regime. The dashed vertical black line indicates the theoretical percolation threshold for the potential seen by tightly bound, pointlike pairs.

disorder dominates over interactions, even in a unitary Fermi gas.

The drop of resistance takes place close to the transition observed in the *in situ* data. This suggests that a percolation process plays a role in the transition: for strong disorder, the superfluid fraction should be localized and transport takes place as if the gas was normal. At the percolation threshold, the superfluid islands start to connect and the resistance drops accordingly. This picture is similar to that of weakly interacting bosons in one dimension, as theoretically investigated in Refs. [39,40]. The classical percolation threshold of the potential for a free atom of energy μ is reached in two dimensions at $\bar{V} = 1.92\mu$ [36,41]. However, the potential seen by pairs is a more intricate problem and in the limit of tightly bound, pointlike pairs, it is equal to twice that for free atoms [38]. In this extreme case, the percolation transition for pairs happens at $\bar{V} = 0.95\mu$. This is indicated by the dashed, vertical lines in Figs. 1(h), 2(c), 2(e), and 3. A reason why the resistance starts to drop slightly later at $\bar{V}/\mu \simeq 0.7$ could be that density distributions are sensitive to pairing and condensation, while currents are sensitive to superfluidity and phase coherence. The latter may in addition be affected by dynamical phenomena like phase slippage.

The interpretation in terms of percolation of pairs is strengthened by the following observations. (i) For $\bar{V}/\mu \gtrsim 1$, the resistance of the thin film is identical to that of weakly interacting, unpaired fermions, suggesting that pairs do not contribute to the transport above this disorder strength. (ii) The *in situ* measurements reveal regions where the density is constant for all disorder strengths. This is only possible if superfluidity is preserved locally, since the normal gas has a significantly lower compressibility [42,43] and could therefore not accommodate the same amount of particles at fixed chemical potential imposed by the reservoirs. (iii) In the percolation analysis leading to Figs. 2(c) and 2(e), the sharp initial drop of the threshold density n_{th} stops at $\bar{V}/\mu \simeq 1$ as expected if pairs are localized at this value. The remaining finite n_{th} for $\bar{V}/\mu > 1$ we attribute to unpaired atoms, the same that give rise to the normal-state transport properties in that regime. (iv) The correlated disorder will naturally increase the binding energy of pairs, localizing them into a single potential minimum. This fact was already pointed out in several theoretical analyses about cold atoms and dirty superconductors [44–48], and emerges naturally for classical disorder, where already at $\bar{V}/\mu \sim 0.3$, we should have $E_b \sim E_\sigma$ (see the Supplemental Material [17]).

While the percolation picture is a plausible candidate for the nature of the fragmented state, the transition from fragmented to superfluid is likely to be influenced by tunneling between isolated clusters, leading to a disordered Josephson junction array [10]. Furthermore, the disorder can also enhance the interaction-induced depletion of the condensate fraction of pairs [49–51]. Eventually, since the thin film is quasi-2D, unbound vortex-antivortex pairs may lead to dissipation before the superfluid cluster disconnects [52].

In the future, the ability to locally observe the density distributions could be extended to a local measurement of the single-particle density of states using radio-frequency spectroscopy. This may allow us to directly relate our findings to prominent models of disordered systems, such as a Bose-glass [2,3], or a pseudogap phase [53].

We acknowledge fruitful discussions with Dima Shepelyanski, Gabriel Lemarié, Thierry Giamarchi, Dan Shahar, Vijay Shenoy, Vincent Josse, Antoine Georges, Corina Kollath, Charles Grenier and Sebastiano Pilati. We acknowledge financing from NCCR MaNEP and NCCR QSIT, the ERC Projects SQMS, the FP7 Projects NAME-QUAM and SIQS, and ETHZ. J. P. B. is supported by the EU through a Marie Curie Fellowship and the Ambizione program of SNSF.

*brantutj@phys.ethz.ch

[1] E. J. Mueller, T.-L. Ho, M. Ueda, and G. Baym, Phys. Rev. A **74**, 033612 (2006).
[2] T. Giamarchi and H. J. Schulz, Phys. Rev. B **37**, 325 (1988).

[3] M. P. A. Fisher, P. B. Weichman, G. Grinstein, and D. S. Fisher, Phys. Rev. B **40**, 546 (1989).
[4] L. Fallani, J. E. Lye, V. Guarrera, C. Fort, and M. Inguscio, Phys. Rev. Lett. **98**, 130404 (2007).
[5] Y. P. Chen, J. Hitchcock, D. Dries, M. Junker, C. Welford, and R. G. Hulet, Phys. Rev. A **77**, 033632 (2008).
[6] M. Pasienski, D. McKay, M. White, and B. DeMarco, Nat. Phys. **6**, 677 (2010).
[7] M. C. Beeler, M. E. W. Reed, T. Hong, and S. L. Rolston, New J. Phys. **14**, 073024 (2012).
[8] B. Allard, T. Plisson, M. Holzmann, G. Salomon, A. Aspect, P. Bouyer, and T. Bourdel, Phys. Rev. A **85**, 033602 (2012).
[9] C. Chin, R. Grimm, P. Julienne, and E. Tiesinga, Rev. Mod. Phys. **82**, 1225 (2010).
[10] V. F. Gantmakher and V. T. Dolgopolov, Fiz. Usp. **53**, 1 (2010).
[11] I. Bloch, J. Dalibard, and W. Zwerger, Rev. Mod. Phys. **80**, 885 (2008).
[12] J.-P. Brantut, J. Meineke, D. Stadler, S. Krinner, and T. Esslinger, Science **337**, 1069 (2012).
[13] D. Stadler, S. Krinner, J. Meineke, J.-P. Brantut, and T. Esslinger, Nature (London) **491**, 736 (2012).
[14] S. Krinner, D. Stadler, J. Meineke, J.-P. Brantut, and T. Esslinger, Phys. Rev. Lett. **110**, 100601 (2013).
[15] B. Fröhlich, M. Feld, E. Vogt, M. Koschorreck, W. Zwerger, and M. Köhl, Phys. Rev. Lett. **106**, 105301 (2011).
[16] A. T. Sommer, L. W. Cheuk, M. J. H. Ku, W. S. Bakr, and M. W. Zwierlein, Phys. Rev. Lett. **108**, 045302 (2012).
[17] See Supplemental Material http://link.aps.org/supplemental/10.1103/PhysRevLett.115.045302 for technical details on the cloud, disordered potential characterisation, resistance measurement and percolation analysis, and for a simple model for scattering in the presence of disorder, which includes Refs. [18–30].
[18] B. Zimmermann, T. Müller, J. Meineke, T. Esslinger, and H. Moritz, New J. Phys. **13**, 043007 (2011).
[19] J. W. Goodman, *Speckle Phenomena in Optics: Theory and Applications* (Roberts and Company, Englewood, 2007).
[20] D. S. Petrov and G. V. Shlyapnikov, Phys. Rev. A **64**, 012706 (2001).
[21] O. Morsch and M. Oberthaler, Rev. Mod. Phys. **78**, 179 (2006).
[22] T. Busch, B.-G. Englert, K. Rzażewski, and M. Wilkens, Found. Phys. **28**, 549 (1998).
[23] Z. Idziaszek and T. Calarco, Phys. Rev. A **71**, 050701 (2005).
[24] T. Giamarchi and H. J. Schulz, Phys. Rev. B **37**, 325 (1988).
[25] H. Gimperlein, S. Wessel, J. Schmiedmayer, and L. Santos, Phys. Rev. Lett. **95**, 170401 (2005).
[26] C. W. Johnson, G. F. Bertsch, and D. J. Dean, Phys. Rev. Lett. **80**, 2749 (1998).
[27] T. Papenbrock, L. Kaplan, and G. F. Bertsch, Phys. Rev. B **65**, 235120 (2002).
[28] P. Jacquod and A. D. Stone, Phys. Rev. Lett. **84**, 3938 (2000).
[29] D. Stauffer and A. Aharony, *Introduction to Percolation Theory* (Taylor & Francis, London, 1994).
[30] J. Levinsen and M. M. Parish, arXiv:1408.2737.
[31] B. Shapiro, J. Phys. A **45**, 143001 (2012).
[32] R. C. Kuhn, O. Sigwarth, C. Miniatura, D. Delande, and C. A. Müller, New J. Phys. **9**, 161 (2007).
[33] B. Shklovskii, Semiconductors **42**, 909 (2008).
[34] A. Frydman, Physica (Amsterdam) **391C**, 189 (2003).
[35] S. Kirkpatrick, Rev. Mod. Phys. **45**, 574 (1973).
[36] L. Pezzé, M. Robert-de-Saint-Vincent, T. Bourdel, J.-P. Brantut, B. Allard, T. Plisson, A. Aspect, P. Bouyer, and L. Sanchez-Palencia, New J. Phys. **13**, 095015 (2011).
[37] R. Zallen and H. Scher, Phys. Rev. B **4**, 4471 (1971).
[38] S. Giorgini, L. P. Pitaevskii, and S. Stringari, Rev. Mod. Phys. **80**, 1215 (2008).
[39] P. Lugan, D. Clement, P. Bouyer, A. Aspect, M. Lewenstein, and L. Sanchez-Palencia, Phys. Rev. Lett. **98**, 170403 (2007).
[40] L. Fontanesi, M. Wouters, and V. Savona, Phys. Rev. A **83**, 033626 (2011).
[41] A. Weinrib, Phys. Rev. B **26**, 1352 (1982).
[42] M. J. H. Ku, A. T. Sommer, L. W. Cheuk, and M. W. Zwierlein, Science **335**, 563 (2012).
[43] N. Navon, S. Nascimbène, X. Leyronas, F. Chevy, and C. Salomon, Phys. Rev. A **88**, 063614 (2013).
[44] J. Lages and D. L. Shepelyansky, Phys. Rev. B **62**, 8665 (2000).
[45] G. Dufour and G. Orso, Phys. Rev. Lett. **109**, 155306 (2012).
[46] F. Palestini and G. C. Strinati, Phys. Rev. B **88**, 174504 (2013).
[47] A. Ghosal, M. Randeria, and N. Trivedi, Phys. Rev. Lett. **81**, 3940 (1998).
[48] K. Bouadim, Y. L. Loh, M. Randeria, and N. Trivedi, Nat. Phys. **7**, 884 (2011).
[49] G. Orso, Phys. Rev. Lett. **99**, 250402 (2007).
[50] C. A. Müller and C. Gaul, New J. Phys. **14**, 075025 (2012).
[51] G. E. Astrakharchik, K. V. Krutitsky, and P. Navez, Phys. Rev. A **87**, 061601 (2013).
[52] G. Carleo, G. Boéris, M. Holzmann, and L. Sanchez-Palencia, Phys. Rev. Lett. **111**, 050406 (2013).
[53] M. V. Feigel'man, L. B. Ioffe, V. E. Kravtsov, and E. Cuevas, Ann. Phys. (Amsterdam) **325**, 1390 (2010).